Journal of Alloys and Compounds 506 (2010) 877–882

Contents lists available at ScienceDirect

Journal of Alloys and Compounds

journal homepage: www.elsevier.com/locate/jallcom

A novel preparation of highly active iron-doped titania photocatalysts with a p–n junction semiconductor structure

Song Liu*, Xingping Liu, Yanshan Chen, Rongying Jiang

Department of Applied Chemistry, South China University of Technology, Guangzhou 510640, PR China

ARTICLE INFO

Article history:
Received 28 November 2009
Received in revised form 10 July 2010
Accepted 13 July 2010
Available online 21 July 2010

Keywords:
TiO_2
Fe
Uneven doping
p–n junction
P25
Inorganic materials

ABSTRACT

Iron (III)-doped TiO_2 powder photocatalysts were prepared by modified uneven doping method using ammonium oleate in order to promote the formation of p–n junction composite structure, and were characterized by X-ray diffraction (XRD), TEM, BET, UV–vis and PL spectroscopy. The photocatalytic activities of TiO_2-based nanoparticles were evaluated by the photocatalytic rate of methyl orange oxidation. These iron (III)-doped TiO_2 photocatalysts are the composite powders having the p–n junction of n-type undoped TiO_2 with p-type TiO_2 doped by Fe evenly, were shown to have a much higher photocatalytic destruction rate than that of undoped TiO_2. The n–n junctions may be responsible for the high photocatalytic activity of P25 and other mix-phase crystalline titania.

1. Introduction

In recent years, titania photocatalyst have attracted much attention as an environmentally harmonious and clean catalyst. However, the efficiency of the photocatalytic degradation reaction is limited by the high recombination rate of photoinduced electrons and holes [1]. The fast recombination is in competition with the reactions decomposing the pollutants. Many scientists tried to solve these problems by changing the electronic structure of the photocatalyst via doping titania with transition metal ions [1]. Among many candidates, iron (III) ion seems to be the promising for this purpose [1–41]. Some investigators reported that doping of iron ion in TiO_2 increased its photocatalytic activity [1–30], though others have shown that Fe doping can reduce photocatalytic activity [31–40]. The photocatalytic activity of iron-doped titania strongly depends on the doping method and the concentration of iron in the photocatalysts. Iron-doped titania samples have been prepared by controlled hydrolysis [1,2,24,40], ultrasonic [3], sol–gel [4–9,20,26,29,30], mechanical alloying [10], co-precipitation [9,11,33,38], hydrothermal [12,25,29,34], microemulsion [13,39], reactive magnetron sputtering [14,15], metal organic chemical vapor deposition [16], combining sol–gel method with hydrothermal treatment [17,35], controlled hydrolysis followed by hydrothermal treatment [18], homogeneous precipitation-hydrothermal [19], hydro-alcohol thermal [21], impregnation [22,31,32], electrochemical anodic oxidation [23], high-pressure crystallization [27], solvothermal [28], plasma oxidative pyrolysis [36] and solution combustion method [37]. Recently, Li et al. prepared metal ions (Mo^{6+} and Ni^{2+}) doped TiO_2 thin films by two kinds of methods of doping, i.e., even doping and uneven doping processes [42–44]. They found uneven doping process was able to improve the photocatalytic activity significantly compared with the traditional process (even doping).

In previous paper [45], we prepared two kinds of iron (III)-doped TiO_2 powder photocatalysts by even doping and uneven doping methods, and found that TiO_2 photocatalysts doped by Fe unevenly with a p–n junction semiconductor structure were shown to have a much higher photocatalytic destruction rate than that of TiO_2 photocatalysts doped by Fe evenly and undoped TiO_2. There were some reports on photocatalyst being combined with p–n semiconductors to improve charge separation that minimizes the energy wasteful electron-hole recombination [46–62].

In the present paper, we prepared the iron-doped TiO_2 powder photocatalysts by a modified uneven doping method using ammonium oleate in order to promote the formation of p–n junction composite structure and found modified uneven doping could enhance the photocatalytic activity greatly. To the best of our knowledge such preparation method (modified uneven doping method) of iron (III)-doped TiO_2 powder has not been reported earlier.

* Corresponding author. Tel.: +86 020 87114875; fax: +86 020 87112906.
E-mail address: chsliu@scut.edu.cn (S. Liu).

0925-8388/$ – see front matter © 2010 Elsevier B.V. All rights reserved.
doi:10.1016/j.jallcom.2010.07.103

Table 1
Samples preparation condition and results.

Sample	Doping mode	Fe/at%[a]	Specific area ($m^2\ g^{-1}$)	Apparent rate constant (min^{-1})
P25	–	0		0.098
Pure TiO_2	–	0	79.7	0.0087
0.065%Fe–TiO_2	Even doping	0.065		0.0081
0.5%Fe–TiO_2	Even doping	0.50	76.4	0.0041
6.7TiO_2/0.5%Fe–TiO_2	Uneven doping	0.065	78.7	0.024
6.7TiO_2/0.5%Fe–TiO_2/M	Modified uneven doping	0.065	69.3	0.12

[a] Content of iron in total uneven and modified uneven doping samples.

2. Experimental

2.1. Preparation

Pure titania catalyst using tetrabutyl titanate as a titanium precursor was synthesized using the sol–gel method at room temperature. 40 mL of absolute ethyl alcohol, 10 mL of glacial acetic acid and 5 mL of double-distilled water were mixed as solution *a*, then it was added drop-wise under vigorous stirring into the solution *b* that contains 17 mL of tetrabutyl titanate and 40 mL of absolute ethyl alcohol. The resulting transparent colloidal dispersion (marked as TiO_2-sol) was stirred for 0.5 h and aged for 2 days till the formation of xerogel, then grounded into powder. The powder was calcined at 400 °C for 3 h, and then grounded in agate mortar to obtain fine titania powders finally.

Several TiO_2 powders doped by Fe evenly (abbreviated hereafter as FeTiE) were generated using the sol–gel method at room temperature by taking precursor $Fe(NO_3)_3{\cdot}9H_2O$ 40 mL of absolute ethyl alcohol, 10 mL of glacial acetic acid and 5 mL of the required concentration of $Fe(NO_3)_3$ solution were mixed as solution *c*, then it was added drop-wise under vigorous stirring into the solution *b*. The following procedures were carried according to the pure titania. The Fe^{3+}–TiO_2 catalysts had a nominal atomic ratio (Fe/Ti) of *x*%, so they are named as *x*%Fe–TiO_2 in this study.

One TiO_2 powder doped by Fe unevenly was generated using the sol–gel method at room temperature with the following procedure: 0.6 g of 0.5%Fe–TiO_2 powders was put into TiO_2-sol under stirring and the resulting suspension was stirred continuously for several days (during the several days, the solvent volatilized slowly). Then, the mixture was dried at 100 °C for 4 h, and fired at 400 °C for 3 h. The as-prepared photocatalysts are named hereafter as 6.7TiO_2/0.5%Fe–TiO_2, 6.7 is the nominal molar ratio of titania of TiO_2-sol to that of 0.5%Fe–TiO_2.

One doped TiO_2 powder was prepared by the modified uneven doping method. Firstly, 3 g 0.5%Fe–TiO_2 powders were sonicated in 30 mL of 0.01 M ammonium oleate aqueous solution (generated by mixing equal moles of ammonia with oleic acid) for 1 h and then stirred for 2 h. Secondly, the solids were separated by centrifugation and washed 3 times with ethanol. The purified powders were dried at 60 °C for 4 h and cooled at room temperature (The as-prepared powders are named hereafter 0.5%Fe–TiO_2–O). Thirdly, 0.6 g of 0.5%Fe–TiO_2–O powders was put into TiO_2-sol under stirring and the resulting suspension was stirred continuously for several days (during the several days, the solvent volatilized slowly). Finally, the mixture was dried at 100 °C for 4 h, and fired at 400 °C for 3 h. The as-prepared photocatalysts are named hereafter as 6.7TiO_2/0.5%Fe–TiO_2/M.

2.2. Characterization

Powder XRD patterns for samples were recorded using a Rigaku Dmax-IIIA diffractometer with Ni-filtered Cu-Kα radiation (λ = 0.154056 nm). The average crystal sizes were calculated from the X-ray diffractograms by the Scherrer formula. A transmission electron microscope (TEM), JEM-2010, was applied to observe the morphology of catalysts and estimate the particle size. The surface area of catalysts was determined using a standard Brunauer–Emmett–Teller (BET) apparatus (Micromeritics TristarII3020). The pore size distribution of the catalysts was determined by the Barrett–Joyner–Halenda (BJH) method. Diffuse reflectance UV/vis spectra were recorded on a Hitachi UV-3010 spectrometer equipped with an integrating sphere of 60 mm in diameter using $BaSO_4$ as a standard. Photoluminescence spectra were collected on a Fluorescence spectrometer (Hitachi F-4500) with a powder holder accessory under room temperature.

2.3. Photoreactivity measurements

Photo decolorization of methyl orange in an aqueous medium was used as a probe reaction to access the photocatalytic activity of all the powders. A Pyrex cylindrical photoreactor with an effective volume of 250 mL was used to conduct photocatalytic degradation experiments, which is surrounded by a Pyrex circulating water jacket. An 8-W UV lamp (Toshiba, Inc.) with a main emission at 365 nm is positioned at the center of the cylindrical vessel and used for photoreaction. For each experiment, 200 mg of photocatalyst was added to 250 mL of 5 mg/L methyl orange solution stirred with a magnetic stirrer. The aerated suspension was first stirred in the dark for 60 min, which was sufficient to reach adsorption equilibrium of methyl orange. The concentration of aqueous methyl orange was determined with a Hitachi UV-3010 spectrometer by measuring the absorbance at 464 nm.

3. Results

3.1. Characterization of photocatalysts

The XRD patterns of TiO_2-based nanoparticles are shown in Fig. 1. The TiO_2 in all the TiO_2-based nanoparticles exist mainly in anatase phase form. The mean crystallite size of pure TiO_2, 0.5%Fe–TiO_2, 6.7TiO_2/0.5%Fe–TiO_2 and 6.7TiO_2/0.5%Fe–TiO_2/M are 13.6, 13.0, 12.4 and 17.2 nm, respectively, indicating that iron modified uneven doping increased the size.

TEM images in Fig. 2 reveal that the prepared samples consisted of aggregates of primary particles of 7–20 nm in diameter. The averaged sizes of pure TiO_2 and 6.7TiO_2/0.5%Fe–TiO_2/M are estimated to be approximately 12 and 17 nm, respectively, which is in general agreement with the XRD determination.

The N_2 adsorption–desorption isotherms of catalysts in Fig. 3 are characteristic type-IV curves according to the BDDT classification with hysteresis loops [63]. The BET surface areas of the photocatalysts are summarized in Table 1. All samples exhibited fairly high surface area in the range of 69–80 $m^2\ g^{-1}$, which were little affected by doping. The BJH pore size distributions (Fig. 4) calculated on the basis of the desorption branches of the isotherms show peaks centered at 7.1, 6.9, 5.4 and 19.5 nm for pure TiO_2, 0.5%Fe–TiO_2, 6.7TiO_2/0.5%Fe–TiO_2 and 6.7TiO_2/0.5%Fe–TiO_2/M, respectively. The formation of mesoporous structure in the samples is attributed to the aggregation of TiO_2 crystallites [20]. There are two probable factors causing the great increase of average pore size for 6.7TiO_2/0.5%Fe–TiO_2/M compared with other samples. One is that larger crystallite aggregation forms larger pores. The other is that the decomposition of ammonium oleate during the process of drying and calcination resulted in a more abundant formation of mesoporous structure.

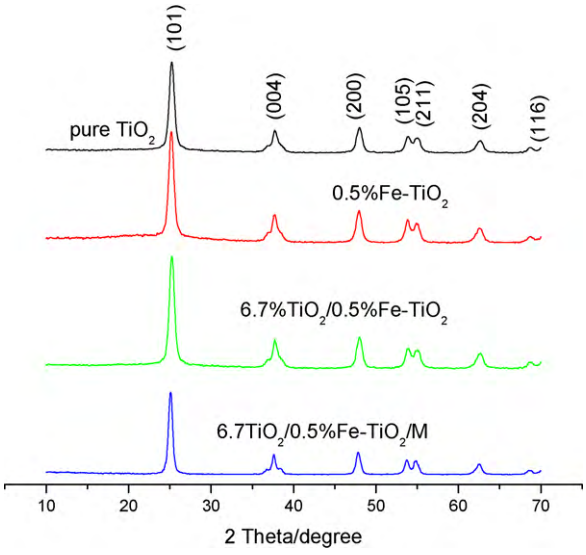

Fig. 1. XRD patterns of catalysts.

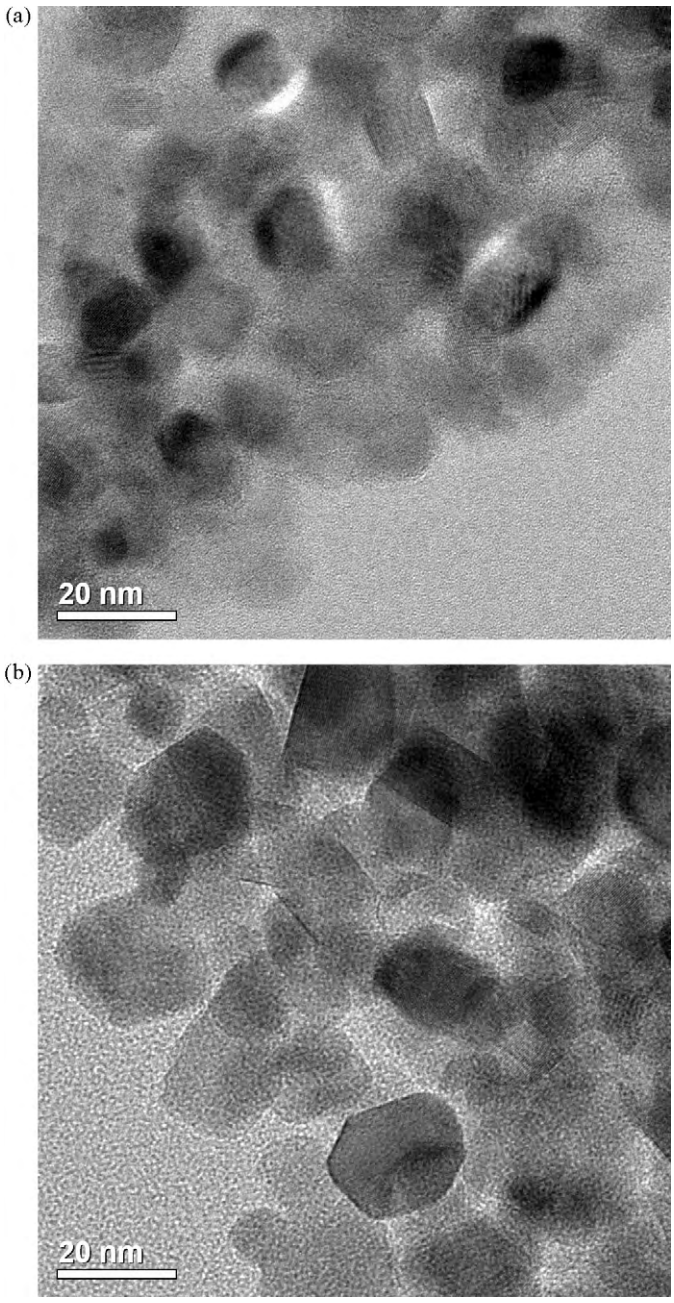

Fig. 2. TEM images of: (a) pure TiO_2 and (b) $6.7TiO_2$/0.5%Fe–TiO_2/M.

UV–vis DRS of TiO_2-based photocatalysts are displayed in Fig. 5. Iron (III)-doping titania showed enhanced absorptions in the range from 400 to 600 nm with increasing Fe content, accompanied with the changes on color from white to reddish yellow.

Photoluminescence spectra of catalysts in Fig. 6 exhibit six main emission peaks at about 399, 422, 452, 469, 483 and 493 nm with excitation at 320 nm. High-energy peaks can be assigned to edge luminescence of the TiO_2 particles, while lower energy peaks are introduced by the presence of the oxygen vacancies [38]. The great decrease in emission intensity of 0.5%V–TiO_2 compared with undoped TiO_2 may be due to the impurity levels introduced by dopant that enhanced non-radiative recombination of the excited electrons [37,64,65]. Similar quenching in the luminescence intensity has also been observed for V-, Fe-, W- Zr-, Cu-, Ni-, Ga-, Cd-, Ag-, Al- and Pb-doped TiO_2 by Nagaveni et al. [37], Zhou et al. [35], Tang et al. [64] and Rahman et al. [65].

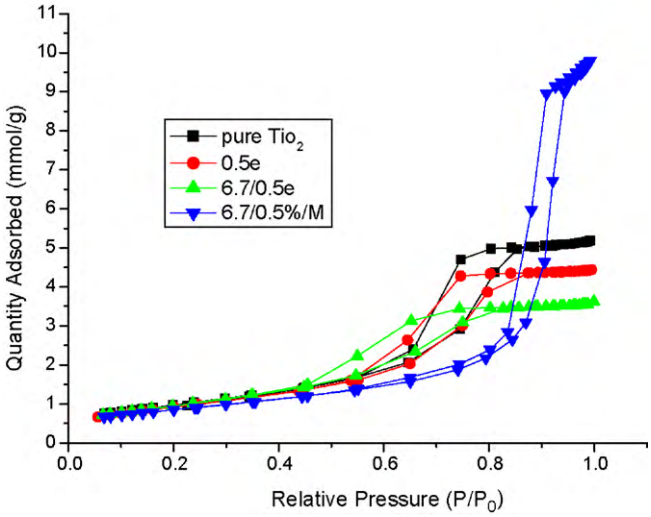

Fig. 3. Nitrogen adsorption–desorption isotherm for photocatalysts.

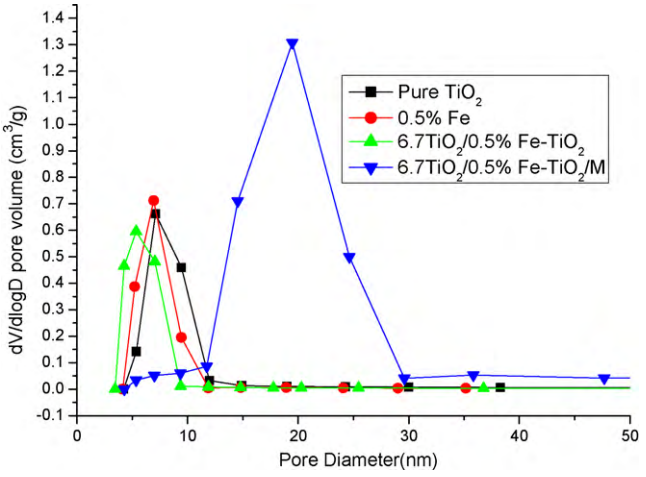

Fig. 4. Pore size distribution curve of photocatalysts.

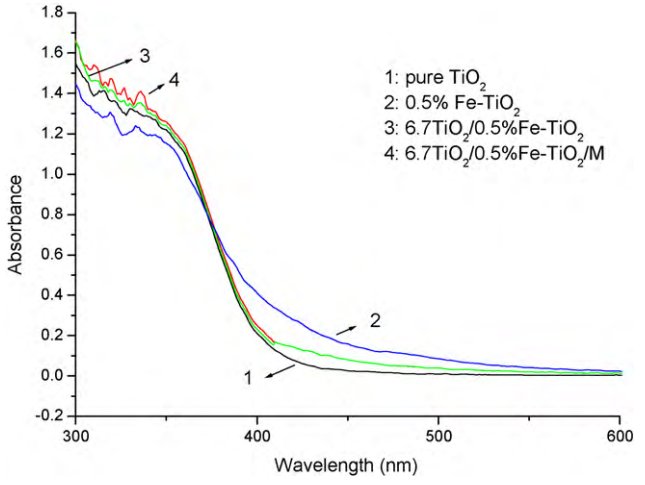

Fig. 5. UV–vis DRS of catalysts.

3.2. Photocatalytic activity

Fig. 7 displays the decrease of methyl orange concentration as a function of UV light irradiation time over TiO_2-based photocata-

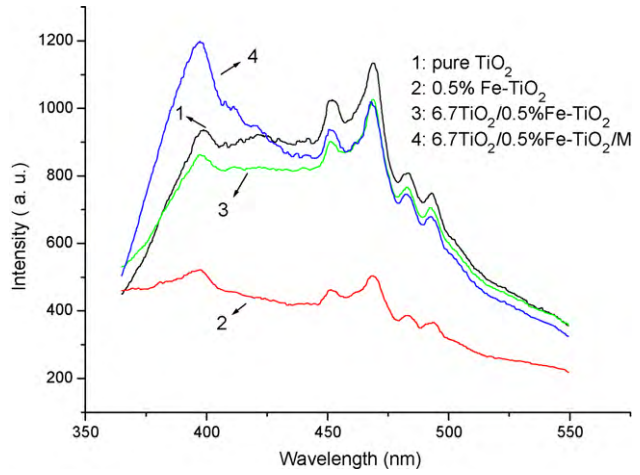

Fig. 6. Photoluminescence emission spectra of photocatalysts with excitation at 320 nm.

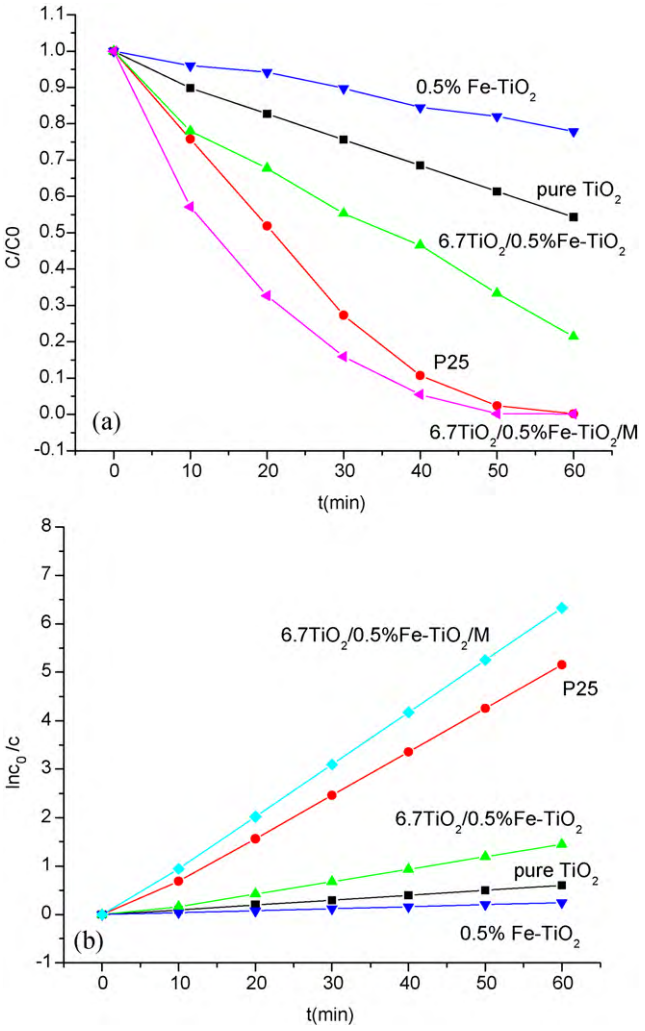

Fig. 7. Decrease of methyl orange concentration as a function of UV irradiation time over the different catalysts.

lysts. The photocatalytic activity of commercial Dugussa P25 TiO_2 catalysts prepared by flame pyrolysis was also included for comparison. The photocatalytic decolorization of methyl orange is an apparent first-order reaction (Fig. 7b). The apparent rate constants of the photocatalysts are displayed in Table 1.

As shown in Fig. 7 and Table 1, it was found that $6.7TiO_2/0.5\%Fe–TiO_2/M$ and $6.7TiO_2/0.5\%Fe–TiO_2$ nanoparticles exhibited much higher photocatalytic activity compared with pure TiO_2 and FeTiE nanoparticles. $6.7TiO_2/0.5\%Fe–TiO_2/M$ had the best photocatalytic activity whose apparent rate constant was about 13.8 times as large as that of pure TiO_2, about 5 times as large as that of $6.7TiO_2/0.5\%Fe–TiO_2$, and about 14.8 times as large as that of $0.065\%Fe–TiO_2$ doped by Fe evenly with the same iron content in the whole iron-doped titania particles as $6.7TiO_2/0.5\%Fe–TiO_2/M$.

4. Discussion

Iron ions can introduce energy levels into the band-gap, which are responsible for the red shift of intrinsic absorption edge of TiO_2 and of the enhancement of visible light adsorption, but there is no direct correlation between the light absorption ability and photocatalytic rate [1–41]. Factors related to the electronic structure seem to be more important, associated to the fact that dopant ions influence charge separation, charge-carrier recombination and interfacial charge-transfer rates, acting as mediators and affecting the quantum efficiencies.

In FeTiE, Fe^{3+} can improve the photocatalytic efficiency by enhancing processes such as separation of photogenerated charges (by hole or electron trapping), detrapping and/or transfer of trapped charges to interface and to adsorbed substrates, reducing consequently recombination [1–41]. However, dopants can act as recombination centers too. The reduced activity can be explained because dopants act more as recombination centers than as trap sites for charge transfer at the interface, especially for the samples with higher Fe^{3+} dopant concentration (sample $0.065\%Fe–TiO_2$ and $0.5\%Fe–TiO_2$) even though these samples have stronger abilities of adsorption and light absorption, which are beneficial to the photoactivity.

In semiconductor devices it is frequently necessary to introduce abrupt discontinuities and graded distributions of different types of doping impurity. An obvious example is the fabrication of p–n junctions [66]. At a p–n junction located at the juncture between p-type and n-type material, electrons diffuse from n-type into p-type region, creating an accumulation of negative charges in the p-type region in the vicinity of the junction. Similarly, holes diffuse from the p-type to n-type region, creating a positive section in the n-type region in the vicinity of the junction. This sets up an internal electrostatic field directed from n-type to p-type region, creating an energy barrier (eV) for the electron transfer from n-type to p-type material. The region in which these carrier densities are nonuniform is known as space-charge region (depletion layer) [46,57,66]. When a p–n junction is formed in a photocatalytic system, the hole-electron pairs, excited by photons, will immediately separate under internal electrostatic field in the p–n junction region and move electrons and holes in opposite directions to minimize recombination and increase photocatalytic activity [46–53]. Some photocatalysts with a p–n junction semiconductor structure and consequent enhanced performances, such as Pt/TiO_2 nanotube [46], p-$CaFe_2O_4$/n-$PbBi_2Nb_{1.9}W_{0.1}O_9$ [47], p-Co_3O_4/n-$BiVO_4$ [48], p-$BaTiO_3$/n-Bi_2O_3 [49], p-$AgGaS_2$/n-CdS [50], p-NiO/n-TiO_2 [51], p-BDD/n-TiO_2 [52,53], nickel-loaded layered perovskite [54], p-$Sr(Zr_{1-x}Y_x)O_{3-\delta}$/n-$TiO_2$ [55], p-$FeTiO_3$/n-TiO_2 [56], p-Se/n-TiO_2 [57,58], p-CoO/n-$SrTiO_3$ [59], p-$CuBi_2O_4$/n-WO_3 [60], p-Co_3O_4/n-Bi_2WO_6 [61] and p-NiO/n-ZnO [62] have been prepared.

Bally et al. [67] have researched structural and electrical properties of pure and Fe-doped TiO_2 thin films. Electrical and thermoelectric power measurements show that the electrical conduction changes from n-type conduction for undoped TiO_2 to p-type conduction for heavily doped (for Fe concentrations larger than 0.13 at.%) and demonstrate that iron atoms behave as accep-

tor impurities. Liau et al. [68] have prepared nano-TiO_2 electrodes by coating Fe-doped TiO_2 film on top of undoped TiO_2 film. It shows that these electrodes give a strong rectifying action, which is the characteristic of a p–n junction. So FeTiE is taken as a p-type semiconductor; whereas titanium dioxide is kind of n-type semiconductor [67,68].

In the process of preparation of $6.7TiO_2$/0.5%Fe–TiO_2 or $6.7TiO_2$/0.5%Fe–TiO_2/M, after the addition of 0.5%Fe–TiO_2 or 0.5%Fe–TiO_2–O into TiO_2-sol, a mixture of 0.5%Fe–TiO_2 with amorphous undoped TiO_2 particles was obtained. In the subsequent process of calcination, amorphous undoped titania crystallized and combined with 0.5%Fe–TiO_2 nanoparticles by sintering. Therefore, at the interfaces between 0.5%Fe–TiO_2 with undoped anatase titania particles, a p–n junction will be formed. Under irradiation, both 0.5%Fe–TiO_2 and undoped anatase titania nanoparticles absorb the band-gap photons and then the electron-hole pairs are generated. Photogenerated holes and electrons separate under the influence of the internal electrostatic field in the p–n junction region. Holes move to 0.5%Fe–TiO_2 side, and electrons to the undoped anatase titania nanoparticles side. Thereby, the chance of electron-hole recombination is reduced. This leads to high photocatalytic activity of photooxidation of methyl orange [47].

The point of zero charge (PZC) of an oxide is the value of pH required to give zero net surface charge. The values of PZC reported for TiO_2, 0.3%Fe–TiO_2, 1%Fe–TiO_2, 2%Fe–TiO_2, and 5%Fe–TiO_2 are 7.1, 7.2, 7.4, 7.7 and 8.1, respectively [32]. The surface of transparent colloidal titania nanoparticles and 0.5%Fe–TiO_2 was positively charged at the pHs in the TiO_2-sol (pH = 4). The surface of 0.5%Fe–TiO_2–O nanoparticles was negatively charged because the oleate anions had been adsorbed onto the surface of 0.5%Fe–TiO_2 nanoparticles. In the case of $6.7TiO_2$/0.5%Fe–TiO_2/M nanoparticles, when 0.5%Fe–TiO_2–O nanoparticles were added into TiO_2-sol, transparent colloidal titania nanoparticles (positively charged) would link up with 0.5%Fe–TiO_2–O nanoparticles (negatively charged) because of electrostatic attraction. After the drying and calcination, amorphous colloidal titania nanoparticles changed into crystalline anatase nanoparticles and at the interface between anatase nanoparticles with 0.5%Fe–TiO_2–O nanoparticles, the p–n junctions would be formed because of the sintering between anatase nanoparticles with 0.5%Fe–TiO_2–O nanoparticles. But in the case of $6.7TiO_2$/0.5%Fe–TiO_2 nanoparticles, when 0.5%Fe–TiO_2 nanoparticles were added into TiO_2-sol, electrostatic repulsion between positively charged colloidal titania nanoparticles with positively charged 0.5%Fe–TiO_2 nanoparticles might obstruct the adhesion of colloidal titania nanoparticles on 0.5%Fe–TiO_2 nanoparticles. So the quantity of p–n junctions of $6.7TiO_2$/0.5%Fe–TiO_2 nanoparticles was less than that of $6.7TiO_2$/0.5%Fe–TiO_2/M nanoparticles and therefore the photocatalytic activity of the former was lower than that of the latter.

As shown in Fig. 7 and Table 1, P25 Degussa commercial powders exhibited good photocatalytic activity, too. P25 is a mixture of rutile and anatase [69,70]. Bickley et al. [69] attributed high photocatalytic activity of the P25 to the presence of rutile and anatase phases in it. Rutile itself is a low-active phase, but the junction created by the two semiconductors helps the charge-carriers separation. The rutile phase of P25 plays the role of charges separation and provides sites for oxidation. Ying et al. [12] proposed that the high photocatalytic activity of the P25 was due to its high crystallinity and a minor Fe^{3+} doping and the photocatalytic activity of the P25 was mainly derived from its anatase phase. Gray et al. [70] thought that the tetrahedral Ti^{4+} sites contributed to the increased photoactivity of the mixed-phase material relative to the pure-phase anatase.

It is well-known that anatase and rutile are both of n-type semiconductors [71,72]. At the interfaces between rutile and anatase, n–n junctions will be formed. Because the Fermi level of anatase is higher than that of rutile [71,72], at a n–n junction located at the juncture between anatase and rutile, electrons diffuse from anatase into rutile region, creating an accumulation of negative charges in the rutile region and a positive section in the anatase region in the vicinity of the junction. This sets up an internal electrostatic field directed from anatase to rutile region, creating an energy barrier (eV) for the electron transfer from anatase to rutile [66]. Under irradiation, both rutile and anatase nanoparticles absorb the band-gap photons and then the electron-hole pairs are generated. Photogenerated holes and electrons separate under the influence of the internal electrostatic field in the n–n junction region. Holes move to rutile side, and electrons to the anatase side. Thereby, the chance of electron-hole recombination is reduced. This leads to high photocatalytic activity of photooxidation of methyl orange, in other words, the n–n junctions may be responsible for the high photocatalytic activity of P25 and other mix-phase crystalline titania [69,70,73–75].

5. Conclusions

Iron (III)-doped TiO_2 powder photocatalysts were prepared by modified uneven doping method using ammonium oleate in order to promote the formation of p–n junction composite structure. These iron (III)-doped TiO_2 photocatalysts are the composite powders having the p–n junction of n-type undoped TiO_2 with p-type TiO_2 doped by Fe evenly, were shown to have a much higher photocatalytic destruction rate than that of undoped TiO_2. $6.7TiO_2$/0.5%Fe–TiO_2/M had the best photocatalytic activity whose apparent rate constant was about 13.8 times as large as that of pure TiO_2, about 5 times as large as that of $6.7TiO_2$/0.5%Fe–TiO_2, and about 14.8 times as large as that of 0.065%Fe–TiO_2 doped by Fe evenly with the same iron content in the whole iron-doped titania particles as $6.7TiO_2$/0.5%Fe–TiO_2/M. The n–n junctions may be responsible for the high photocatalytic activity of P25 and other mix-phase crystalline titania.

References

[1] W.Y. Choi, A. Termin, M.R. Hoffmann, J. Phys. Chem. B 98 (1994) 13669.
[2] C.Y. Wang, C. Bottcher, D.W. Bahnemann, J.K. Dohrmann, J. Mater. Chem. 13 (2003) 2322.
[3] M.H. Zhou, J.G. Yu, B. Cheng, J. Hazard. Mater. B 137 (2006) 1838.
[4] A. Kumbhar, G. Chumanov, J. Nanoparticle Res. 7 (2005) 489.
[5] J.Y. Feng, R.S.K. Wong, X.J. Hu, P.L. Yue, Catal. Today 98 (2004) 441.
[6] J.W. Shi, J.T. Zheng, Y. Hu, Y.C. Zhao, Mater. Chem. Phys. 106 (2007) 247.
[7] B.F. Xin, Z.Y. Ren, P. Wang, J. Liu, L.Q. Jing, H.G. Fu, Appl. Surf. Sci. 253 (2007) 4390.
[8] W.C. Hung, S.H. Fu, J.J. Tseng, H. Chu, T.H. Ko, Chemosphere 66 (2007) 2142.
[9] K.T. Ranjit, B. Viswanathan, J. Photochem. Photobiol. A 108 (1997) 79.
[10] J.H. Jho, D.H. Kim, S.J. Kim, K.S. Lee, J. Alloy Compd. 459 (2008) 386.
[11] Z. Ambrus, N. Balazs, T. Alapi, G. Wittmann, P. Slipos, A. Dombi, K. Mogyorosi, Appl. Catal. B 81 (2008) 27.
[12] Z.B. Zhang, C.C. Wang, R. Zakaria, J.Y. Ying, J. Phys. Chem. B 102 (1998) 10871.
[13] C. Adn, A. Bahamonde, M. Fernndez-Garea, A. Martnez-Arias, Appl. Catal. B 72 (2007) 11.
[14] W.J. Zhang, Y. Li, S.L. Zhu, F.H. Wang, Chem. Phys. Lett. 373 (2003) 333.
[15] J.O. Carneiro, V. Teixeira, A. Portinha, L. Dupk, A. Magalhaes, P. Coutinhu, Vacuum 78 (2005) 37.
[16] X.W. Zhang, M.H. Zhou, L. Lei, Catal. Commun. 7 (2006) 427.
[17] J.F. Zhu, F. Chen, J.L. Zhang, H.J. Chen, M. Anpo, J. Photochem. Photobiol. A 180 (2006) 196.
[18] T.Z. Tong, J.L. Zhang, B.Z. Tian, F. Chen, A. He, J. Hazard. Mater. 155 (2008) 572.
[19] Y. Cong, J.L. Zhang, F. Chen, M. Anpo, D. He, J. Phys. Chem. C 111 (2007) 10618.
[20] M.H. Zhou, J.G. Yu, B. Cheng, H.G. Yu, Mater. Chem. Phys. 93 (2005) 159.
[21] J. Li, J. Xu, W. Dai, H. Li, K. Fan, Appl. Catal. B 85 (2009) 162.
[22] N. Murakami, T. Chiyoya, T. Tsubota, T. Ohno, Appl. Catal. A 348 (2008) 148.
[23] L. Sun, J. Li, C.L. Wang, S.F. Li, H.B. Chen, C.J. Lin, Sol. Energy Mater. C 93 (2009) 1875.
[24] K. Melghit, O.S. Al-Shukeili, I. Al-Amri, Ceram. Int. 35 (2009) 433.
[25] P. Viljayan, C. Mahendiran, C. Suresh, K. Shanthi, Catal. Today 141 (2009) 220.
[26] W.C. Hung, Y.C. Chen, H. Chu, J.J. Tseng, Appl. Surf. Sci. 253 (2008) 2205.
[27] C.H. Lu, C.Y. Hu, C.H. Wu, J. Hazard. Mater. 159 (2008) 636.
[28] M. Kang, J. Mol. Cat. A: Chem. 197 (2003) 173.
[29] L. Deng, S. Wang, D. Liu, B. Zhu, W. Huang, S. Wu, S. Zhang, Catal. Lett. 129 (2009) 513.

[30] M. Popa, L. Diamandescu, F. Vasiliu, C.M. Teodorescu, V. Cosoveanu, M. Baia, M. Feder, L. Baia, V. Danciu, J. Mater. Sci. 44 (2009) 358.
[31] J.A. Navio, J.J. Testa, P. Djedjeian, J.R. Padron, D. Rodriguez, M.I. Litter, Appl. Catal. A 178 (1999) 191.
[32] A. Di Paola, G. Marci, L. Palmisano, M. Schiavello, K. Uosaki, B. Ohtani, J. Phys. Chem. B 106 (2002) 637.
[33] S.M. Karvinen, Ind. Eng. Chem. Res. 42 (2003) 1035.
[34] Z.J. Li, W.Z. Shen, W.S. He, X.T. Zu, J. Hazard. Mater. 155 (2008) 590.
[35] J.K. Zhou, Y.X. Zhang, X.S. Zhan, A.K. Ray, Ind. Eng. Chem. Res. 45 (2006) 3503.
[36] X.H. Wang, J.G. Li, H. Kamiyama, Y. Moriyoshi, T. Ishigaki, J. Phys. Chem. B 110 (2006) 6804.
[37] K. Nagaveni, M.S. Hegde, G. Madras, J. Phys. Chem. B 108 (2004) 20204.
[38] N.D. Abazovic, L. Mirenghi, I.A. Jankovic, N. Bibic, D.V. Sojic, B.F. Abramovic, M.I. Comor, Nanoscale Res. Lett. 4 (2009) 518.
[39] A. Fuerte, M.D. Hernandez-Alonso, A.J. Martinez-Arias, M. Fernndez-Garea, J.C. Conesa, J. Soria, Chem. Commun. (2001) 2718.
[40] N. Serpone, D. Lawless, J. Disdier, J.M. Herrmann, Langmuir 10 (1994) 643.
[41] M.I. Litter, J.A. Navfo, J. Photochem. Photobiol. A 98 (1996), 171, and references therein.
[42] J.Y. Zheng, H. Yu, X.J. Li, S.Q. Zhang, Appl. Surf. Sci. 254 (2008) 1630.
[43] Y. Yang, X.J. Li, J.T. Chen, L.Y. Wang, J. Photochem. Photobiol. A 163 (2004) 517.
[44] H. Yu, X.J. Li, S.J. Zheng, W. Xu, Mater. Chem. Phys. 97 (2006) 59.
[45] S. Liu, Y. Chen, Catal. Commun. 10 (2009) 894.
[46] Y.S. Chen, J.C. Crittenden, S. Hackney, L. Sutter, A.W. Hand, Environ. Sci. Technol. 39 (2005) 1201.
[47] H.G. Kim, P.H. Borse, W. Choi, J.S. Lee, Angew. Chem. Int. Ed. 44 (2005) 4585.
[48] M. Long, W. Cai, J. Cai, B. Zhou, X. Chai, Y. Wu, J. Phys. Chem. B 110 (2006) 20211.
[49] X. Lin, J. Xing, W. Wang, Z. Shan, F. Xu, F. Huang, J. Phys. Chem. C 111 (2007) 18288.
[50] J.S. Jang, D.W. Hwang, J.S. Lee, Catal. Today 120 (2005) 174.
[51] S. Chen, S. Zhang, W. Liu, W. Zhao, J. Hazard. Mater. 155 (2008) 320.
[52] J. Qu, X. Zhao, Environ. Sci. Technol. 42 (2008) 4934.
[53] H. Yu, S. Chen, X. Quan, H. Zhao, Y. Zhang, Environ. Sci. Technol. 42 (2008) 3791.
[54] D.W. Hwang, K.Y. Cha, J. Kim, H.G. Kim, S.W. Bae, J.S. Lee, Ind. Eng. Chem. Res. 42 (2003) 1184.
[55] T. Omata, S. Otsuka-Yao-Matsuo, J. Photochem. Photobiol. A: Chem. 156 (2003) 243.
[56] F. Ye, A. Ohmori, C. Li, J. Mater. Sci. 39 (2004) 353.
[57] T.T.Y. Tan, M. Zaw, D. Beydoun, R. Amal, J. Nanoparticle Res. 4 (2002) 541.
[58] N.R. Tacconi, C.R. Chenthamarakshan, K. Rajeshwar, E.J. Tacconi, J. Phys. Chem. B 109 (2005) 11953.
[59] Y. Qin, G. Wang, Y. Wang, Catal. Commun. 8 (2007) 926.
[60] T. Arai, M. Yanagida, Y. Konishi, Y. Iwasaki, H. Sugihara, K. Sayama, J. Phys. Chem. C 111 (2007) 7574.
[61] Q. Xiao, J. Zhang, C. Xiao, X. Tan, Catal. Commun. 9 (2008) 1247.
[62] S. Chen, W. Zhao, W. Liu, S. Zhang, J. Sol–Gel Sci. Technol. 50 (2009) 387.
[63] S.L. Gregg, K.S.W. Sing, Adsorption Surface Area and Porosity, Academic Press, London, 1982.
[64] H. Tang, H. Berger, P.E. Schmid, F. Levy, Solid State Commun. 87 (1993) 847.
[65] M.M. Rahman, K.M. Krishna, T. Soga, T. Jimbo, M. Umeno, J. Phys. Chem. Soilds 60 (1999) 201.
[66] R.A. Smith, Semiconductors, second ed., Cambridge University Press, London, 1978.
[67] A.R. Bally, E.N. Korobeinikova, P.E. Schmid, F.L. Levy, F. Bussy, J. Phys. D 31 (1998) 1149.
[68] L.C. Liau, C.C. Lin, Appl. Surf. Sci. 253 (2007) 8798.
[69] R.I. Bickley, T. Gonzalez-Carreno, J.S. Lees, L. Palmisano, R.J.D. Tilley, J. Solid State Chem. 92 (1991) 178.
[70] G. Li, N.M. Dimitrijevic, L. Chen, J.M. Nichols, T. Rajh, K.A. Gray, J. Am. Chem. Soc. 130 (2008) 5402.
[71] H.P. Maruska, A.K. Ghosh, Sol. Energy 20 (1978) 443.
[72] M. Gratzel, F.P. Rotzinger, Chem. Phys. Lett. 118 (1985) 474.
[73] J. Zhang, Q. Xu, Z. Feng, M. Li, C. Li, Angew. Chem. Int. Ed. 47 (2008) 1766.
[74] A. Zachariah, K.V. Baiju, S. Shukla, K.S. Deepa, J. James, K.G.K. Warrier, J. Phys. Chem. C 112 (2008) 11345.
[75] T. Kawahara, Y. Konishi, H. Tada, N. Tohge, J. Nishii, S. Ito, Angew. Chem. Int. Ed. 41 (2002) 2811.